SSRG International Journal of Electrical and Electronics Engineering
ISSN: 2348-8379/ https://doi.org/10.14445/23488379/IJEEE-V11I4P104

Volume 11 Issue 4, 25-35, April 2024
© 2024 Seventh Sense Research Group®

Original Article

Enhancing Power Quality in Distributed Generation Systems through Hybrid Active Power Filtering and Intelligent Control

P. Purnachander Rao[1], K. Prakash[2], M. Suryakalavathi[3]

[1,3]*Electrical and Electronics Engineering, JNTUH, Hyderabad, India.*
[2]*Electrical and Electronics Engineering, Vaagdevi College of Engineering, Telangana, India.*

[1]*Corresponding Author : purnachander216@gmail.com*

Received: 04 February 2024 Revised: 04 March 2024 Accepted: 03 April 2024 Published: 30 April 2024

Abstract *- The integration of distributed generation, such as PV systems, into power grids has become increasingly popular due to its environmental benefits and potential to reduce dependence on traditional fossil fuel-based generation. However, the intermittent nature of Renewable Energy Sources (RES) like PV introduces challenges related to Power Quality (PQ), including voltage and current harmonics, which can adversely impact the stability and efficiency of the grid. To address these challenges, this study proposes the use of a Hybrid Active Power Filter (HAPF), which is being able to mitigate harmonic distortions and reactive power issues and stabilize the voltage in the distribution system. The proposed HAPF is energized by a PV system-fed high-gain Interleaved Luo Converter, which offers high efficiency and improved power conversion capabilities. A Recurrent Neural Network (RNN) based harmonic extraction technique is introduced to accurately identify and quantify harmonic components in the system's voltage and current waveforms. The RNN provides an intelligent solution to adaptively extract harmonic information and facilitate precise control of the HAPF. The proposed system is simulated in MATLAB, and the results demonstrate that the RNN-based harmonic extraction in conjunction with the HAPFs energized by a PV system-fed high-gain Interleaved Luo (I-Luo) Converter significantly enhances power quality in the distributed generation system in which THD value is 1.96% which shows little harmonic distortion entering the grid.*

Keywords *- PV, RNN, HAPF, MSSO, I-Luo converter.*

1. Introduction

Because of the rising integration of distributed RESs into the utility grid, PQ of Distributed Generation Systems (DGSs) has become a major concern as modules for integrating RESs into utility grids, grid-connected converter architectures, and control methodologies have been thoroughly studied [1, 2]. Local loads' reactive, harmonic, and imbalanced currents can cause instabilities in a DGS because of harmonic resonant frequencies and worsen the PQ at the Point of Common Coupling (PCC) [3].

To deal with these challenges, often two solutions are employed. One focuses on utilizing advanced control techniques for improving grid-connected converters' potential to operate uninterruptedly under unusual utility situations and to enhance the output current waveforms [4]. However, this approach might not be able to completely eliminate the DGSs' impact on the existing subpar power quality. The second method involves using specific PQ conditioners to address the issue of power quality. Yet, the application of passive filters cannot ensure the intended outcomes because of the undesirable resonance found in HV circuits. In the case of passive filters, the compensation implementation is also set. Since active power filters do not have resonance problems and can reduce system harmonics, they are preferred over passive power filters.

Meanwhile, using active filters to remove harmonics is highly expensive. The best option for harmonic reduction has thus been defined as a hybrid active filter, an intermediary solution (between passive and active filters) [5-8]. We discuss the application of HAPF for harmonic removal in electrical distribution networks in this study.

The HAPF serves as a key component in achieving improved PQ by actively compensating for undesired harmonics and reactive power components. Additionally, the proposed solution aims to ensure compliance with LVRT requirements, which are crucial for grid stability during transient conditions. A noteworthy innovation in this study is the application of RNN for accurate harmonic extraction. This technique empowers the system to intelligently and adaptively

This is an open access article under the CC BY-NC-ND license (http://creativecommons.org/licenses/by-nc-nd/4.0/)

extract harmonic information from voltage and current waveforms, contributing to the precise control of the HAPF.

On the other hand, either an active or passive conditioner requires the installation of an additional device. As a result, there will always be negative effects like a greater price, power rating, dimensions, and man-hours. Regarding the standpoint of DGSs, certain grid-connected power conversion devices provide additional capabilities including reactive power adjustment, distortions suppression, and unequal energy modifications that could serve as beneficial supplementary functions for enhancing PQ.

By providing additional amenities to the electrical grid as a high-degree method of integrating RESs, DGSs built around electrical components have the potential to play an important part in LV network distribution. For such extra facilities, an understanding of these grid-connected converters is required. Given examples of hierarchy systems of control, it is proposed that power converters in DGSs operate either in grid-feeding mode or grid-supporting mode [9-14].

Utilizing a renewable-based energy supply structure, notably PV-powered systems, is the most frequently advocated remedy for this. Residential PV system implementation is widespread for a number of reasons. One factor is the price of PV, for instance, which has dropped significantly over the past few years and may continue to do so. Another sign that PVs are going to dominate DG in the upcoming years is the fact that there is a lot of research being done to increase the efficiency of PVs. In contrast, a sudden rise in sunlight may cause the output current of the PV array to rise, necessitating the use of a converter [14-17].

Due to their dependability, affordability, and straightforward design, single-stage converters such as Buck, Boost, Buck-Boost, SEPIC, and LUO converters have traditionally been employed as DC-DC converters to transform fixed DC supplies into variable DC supplies. The aforementioned converters, however, have low efficiency, high ripples, and oscillating source and load current.

I-Luo converters have been suggested as a solution to these issues in order to increase efficiency and decrease ripples. The well-known class of meta-heuristics known as MSSO, which takes its cue from squirrels, is used in this work. To enhance the energy flow of a grid-integrated PV system, a high-gain I-Luo Converter and a PI controller based on the MSSO algorithm are used in this paper. The study introduces the concept of HAPF as a pivotal component in enhancing PQ in distributed generation systems. The HAPF is designed to actively mitigate harmonic distortions, reactive power fluctuations, and voltage instability, thus addressing PQ challenges associated with integrating RESs like PV systems into power grids. Moreover, the proposed work also includes,

- A high-gain Interleaved Luo Converter that enhances the efficiency of power conversion from the PV system.
- A novel approach to control is presented through the introduction of an MSSO-based PI controller.
- An advanced RNN-based technique for accurate harmonic extraction from voltage and current waveforms is introduced in this work. This intelligent approach enables the system to extract harmonic information adaptively, facilitating precise control of the HAPF.
- A strong emphasis is placed on grid stability during transient conditions by ensuring compliance with LVRT requirements.

The proposed work contributes to the field of DGSs by introducing innovative approaches to power quality enhancement. Moreover, the efficacy of the proposed system is rigorously validated through simulations conducted in the MATLAB environment.

2. Proposed System

By assuring that the PV System operates in a resilient manner, the suggested system aims to satisfy the demand for nonlinear loads. The PV array, I-Luo converter, Modified Squirrel-based PI controller, and HAPF are just a few of the components that were taken into consideration when designing the system. Figure 1 depicts the basic circuit design of the suggested solar PV-based systems.

An I-Luo converter is employed in the suggested system to increase output while minimizing switching losses from the PV array's produced electricity. A PI controller with MSSA-tuned parameters is used to keep the I-Luo converter's output voltage at a constant level. Utilizing an optimization method, the I-Luo converter has the advantage of reducing switching losses and improving output voltage stability.

The MSSO-PI controller has a decent chance of solving the maximum peak overshoot issue when compared to the traditional PI controller. The converter achieves steady-state without exceeding the predetermined value by using an adequately calibrated PI controller. It should be pointed out that solar PV systems are maintained with power ratings over their maximum rated capacities, allowing for coupling of the extra power to the grid for usage by neighboring businesses and household customers.

Detuning impacts and failures were also taken into account by creating restrictions during the optimum management, which increased the dependability and applicability of the developed filters. HAPF based on RNN is employed to reduce harmonics while enhancing the power factor in distribution systems. The following sections give a comprehensive justification of the proposed system's architecture and execution.

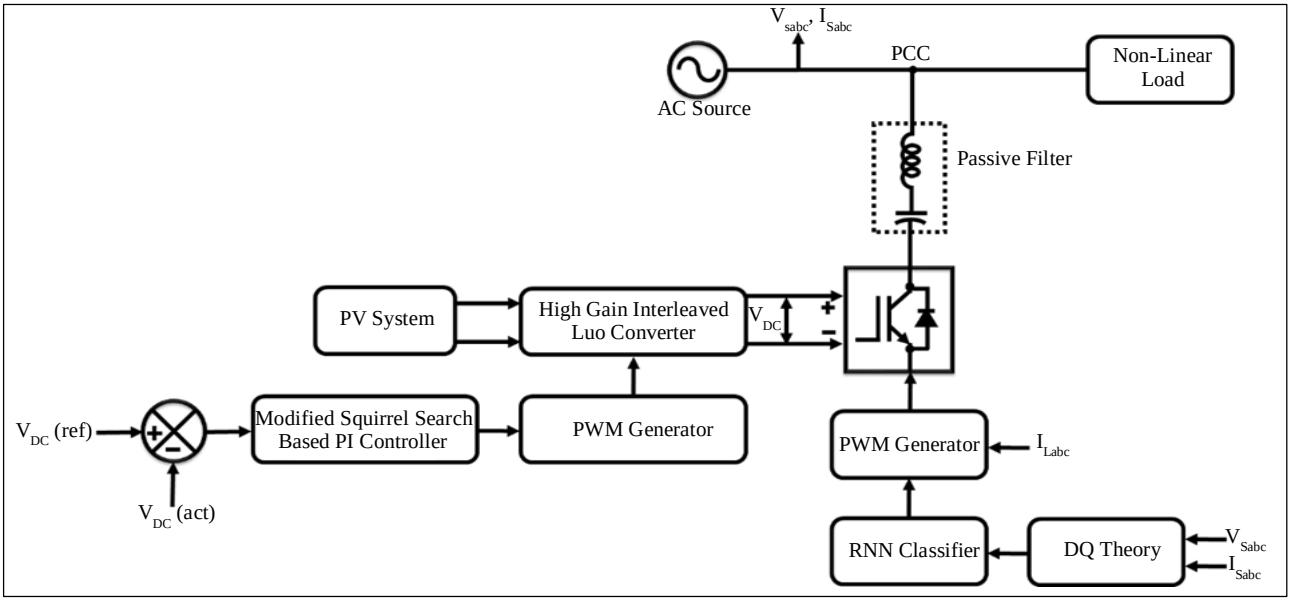

Fig. 1 Basic configuration of hybrid active power filter

3. Modelling of the Work

3.1. Design of PV Array

The PV system's equivalent circuit is depicted in Figure 2 as follows. It is clear from Figure 2 that the PV cell's results are dependent on its input characteristics. Here, I_D is the amount of current passing through the diode; I and V stand for the output current and voltage, whereas R_p and R_s stand for the series and parallel resistance. The solar cell's input current is known as I_{PV} .

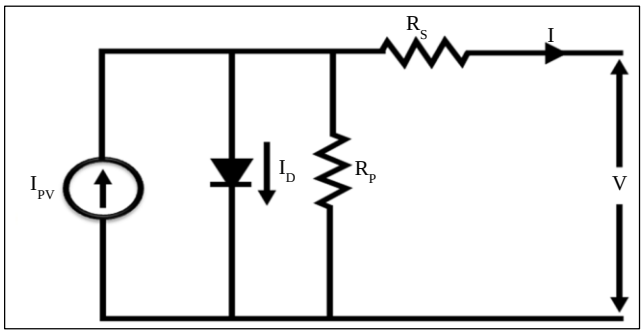

Fig. 2 Equivalent circuit PV cell

Equations 1 and 2 illustrate that the PV cell's output current varies depending on the input cell current, temperature voltage, the PV cell's output voltage, and resistance.

$$I = I_{PVcell} - I_{scell}[exp\frac{(qv)}{\alpha KT} - 1] \quad (1)$$

$$I = I_{PV} - I_0\left[exp\frac{(v+R_S.I)q}{\alpha V_k} - 1\right] - \frac{(v+R_S.I)}{R_p} \quad (2)$$

Equation 2's representation of current output is for a single PV cell. With the PV module arrangement, this can be expressed as Equation 3 illustrates. Typically, this is dependent on N_s, or the quantity of PV cells linked in series.

$$I = I_{PV} - I_0\left[exp\frac{(v+R_S.I)q}{\alpha KT.N_S} - 1\right] - \frac{(v+R_S.I)}{R_p} \quad (3)$$

It is clear from Equation 3 that the PV array's current-to-voltage (I-V) relation is nonlinear, which is caused by changes in incoming solar insolation and increases in the PV array temperature. To get the most PV output power, it is crucial to consider the ideal working area. If the array resistance and the load resistance are equal, the solar PV array produces its maximum power. The positive I-LUO converter receives the PV panel's recovered output power.

3.2. Interleaved Luo Converter

To get minimal output distortion and excellent voltage transfer efficiency of PV energy are made possible with the aid of the I-Luo converter. Figure 3 shows the converter's planned circuit. Simulink-based simulation is used to assess the I-Luo converter's efficiency under varying illumination.

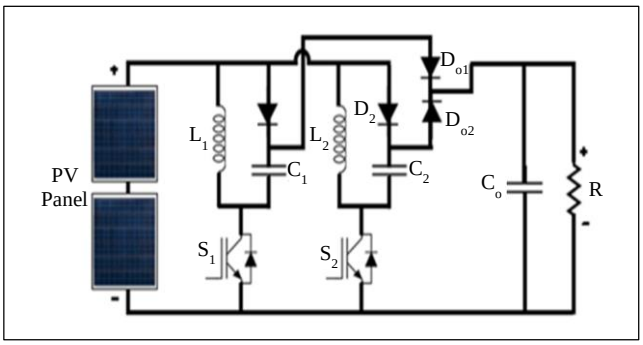

Fig. 3 I-Luo converter circuit

Equation 4 expresses the converter's output voltage, which is V_0 .

$$V_0 = 3\frac{2-d}{1-d}V_{PV} \quad (4)$$

Where V_{PV} , the PV array's output voltage and d is the converter's duty cycle. If the PV's output voltage is at its lowest, a high operating cycle might be required. A power switch, a capacitor, and an inductor make up the I-Luo converter. Equation 5 illustrates that only 40% of ripple current can be allowed when an inductor is used. As a result, the issue of output ripple current can be reduced.

$$\Delta I_L = I_L \times 40\% = I_0 \frac{(V_0 \times 40\%)}{V_{PV}(\min)} \quad (5)$$

The nominal values of L_1 *and* L_2 can be calculated using Equation 6 as follows:

$$L_1, L_2 = \frac{V_{PV}(\min)}{\Delta I_L \times f_{sw}} . dmax \quad (6)$$

Where $dmax$ represents the pulse's highest duty cycle when applied to an I-Luo converter. Equation 7 can be used to get the current's input RMS value:

$$I_{Cin}(rms) = \frac{\Delta I_L}{\sqrt{12}} \quad (7)$$

As demonstrated in Equation 8, the output current is instantly transferred to the output capacitor when the Switch is ON, electrifying the inductor.

$$I_{C0}(rms) = I_0 \sqrt{\frac{V_{DC}+V_D}{V_{PV}(\min)}} \quad (8)$$

Where V_D is the voltage drop between diodes D_1 and D_{01} and V_{DC} is the converter's output voltage. Equation (9), which gives the resulting capacitance value, can be used to calculate it.

$$C_0 = \frac{I_0 \times d}{V_{ripple} X_{0.5} X_{fsw}} \quad (9)$$

Where $X_{0.5}$ *and* X_{fsw} are the impedance at 50% duty cycle and switching frequency, respectively, and d is the PWM pulse duty cycle.

3.3. Modified Squirrel Search Optimization (MSSO) Algorithm Tuned PI Controller

The MSSO, a ground-breaking optimization method, assumes that the search region contains (n) squirrels that fly and (n) deciduous trees. Each flying squirrel only has one tree, and they search through them in order. Three sorts of tree types are distinguished: normal, oak or acorn nuts, and hickory. The final assumption is that three of the trees and one of the trees is an oak tree. The following definition describes the location vector for each *ith* flying squirrel.

$$Fs_i = (Fs_{i1}, Fs_{i2}, \dots, Fs_{id}), (i = 1,2, \dots, n) \quad (10)$$

Every flying squirrel's size is Fs_{ij} , and its beginning location is,

$$Fs_i = Fs_L + U(0,1) * Fs_U - Fs_L \quad (11)$$

Where U(0,1) is a value chosen at random from [0, 1] and Fs_U, Fs_L are the upper and lower search boundaries. The fitness values for the people will be arranged in ascending order, with hickory trees serving as the least value, followed by acorn trees on the other three minimum numbers, and normal trees for the remaining trees. Predators in the forest have a Pdp probability of being there, which affects how individuals migrate to locate food. If there are no predators in the forest, there are three categories for how individuals find food:

$$FS_{at}^{t+1} = \begin{cases} FS_{at}^t + d_g * G_c * FS_{ht}^t - FS_{at}^t) R_1 \geq Pdp \\ Random\ Location\ others \end{cases} \quad (12)$$

R_1 is a random number between [0,1] utilized to maintain equilibrium between the exploration and exploitation modes. Flying squirrels will transition from conventional trees to acorn trees, taking the following new position:

$$FS_{nt}^{t+1} = \begin{cases} FS_{nt}^t + d_g * G_c * FS_{at}^t - FS_{nt}^t) R_2 \geq Pdp \\ Random\ Location\ others \end{cases} \quad (13)$$

R_2 has a value drawn at random from [0, 1]. Flying squirrels may transition from hickory trees to conventional trees, changing their location to:

$$FS_{nt}^{t+1} = \begin{cases} FS_{nt}^t + d_g * G_c * FS_{ht}^t - FS_{nt}^t) R_3 \geq Pdp \\ Random\ Location\ others \end{cases} \quad (14)$$

R_3 also has a random value in the [0, 1] range. The gliding distance and angle are shown in (21) as follows:

$$d_g = \frac{h_g}{\tan(\varphi) * sf} \quad (15)$$

$$\tan(\varphi) = \frac{D}{L} \quad (16)$$

$$D = \frac{1}{2\rho V^2 S C_D} \quad (17)$$

$$D = \frac{1}{2\rho V^2 S C_L} \quad (18)$$

$$S_t^t = \sqrt{\sum_{k=1}^{D} S_{ai,k}^t - S_{h,k}^t \;\; i = 1,2, \dots, Nfs} \quad (19)$$

Some squirrels could not find food at the conclusion of the winter season, so they had to look in other places. These squirrels moved, as shown in (20),

$$FS_{inew}^{t+} = Fs_L + Levy(n) * (Fs_U - Fs_L) \quad (20)$$

Where,

$$Levy(n) = 0.01 * \frac{r_2 \sigma}{|r_b|^{\frac{1}{\beta}}} \quad (21)$$

(n) = (n 1), r_a and r_b are two random numbers between [0, 1], and is a constant value of 1.5. Last but not least, in order to get the best system efficiency, it is necessary to choose a suitable set of fitness criteria. The parameter specifications of MSSO tuned PI controller are provided in Table 1. The SSA method uses the ITAE in (22) as a measure of fitness parameter.

$$ITA = \int |e| \, dt \quad (22)$$

Once the squirrels' locations are updated based on migration and possible Levy Flight, the algorithm calculates the control efforts for each squirrel. This entails computing the error between the reference and actual voltages, followed by generating proportional and integral terms using the PI controller's gains. The resultant control effort represents an adjustment to the converter's switching operation. The application of calculated control efforts to the Interleaved Luo Converter induces adjustments in its switching logic. This dynamic adaptation of the switching operation aims to steer the actual output voltage closer to the desired reference voltage.

3.4. Hybrid Active Power Filter

An active filter and a passive filter are combined to create a HAPF, as seen in Figure 4. It is made up of a static power converter, a passive filter, and a control block that has the ability to govern the complete hybrid filter. Although the active filter is employed to decrease the effectiveness of the power converter and correct for low-frequency harmonic currents produced by the damaging nonlinear load, the passive filter tries to do the same for higher-frequency harmonics.

The benefits of HAPF over conventional filtering components include the ability to resolve issues with nearby harmonic current infusion and resonances, in addition to the fact that the converter's capability is lower than that of a regular active power filter. A more effective way to lower the cost of active power filters is by the use of HAPF.

The hybrid filter must be chosen in accordance with a number of criteria in order to work more effectively, including the filter's structure, the control strategy (RNN) employed, the type of filter utilized in the control loop, and the size of the components that make up the filter.

The methodology employed for designing the primary components within the HAPF is outlined in the following sections.

3.4.1. LC Filter Resonant Frequency (f_r):

Selecting the resonant frequency (f_r) of the LC filter entails the task of identifying the frequency at which the inherent resonance of the inductance (L_f) and capacitance (C_f) components within the filter system become pronounced.

$$f_r = \frac{1}{2\pi\sqrt{L_f C_f}} \quad (23)$$

Ideally, the resonant frequency is chosen in proximity to the primary frequency of the load current harmonic that requires compensation. Given that a single-tuned passive filter is employed, the key consideration in selecting the resonant frequency is to reduce the impedance encountered by the load current harmonics targeted for compensation.

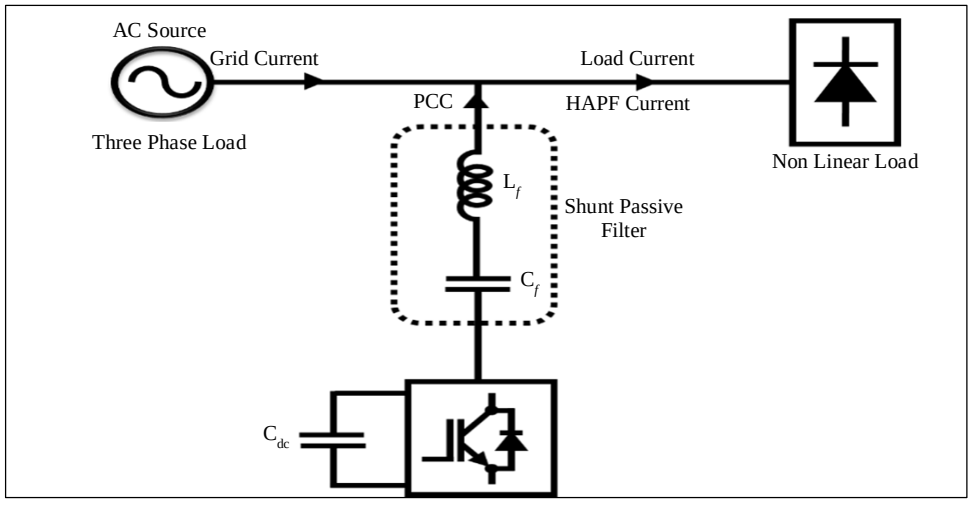

Fig. 4 Structure of HAPF

3.4.2. Design of L_f and C_f

The determination of suitable values for L_f and C_f involves a complex interplay of multiple considerations. An essential objective is to ensure that the Passive Power Filter (PPF) maintains minimal impedance at the harmonic frequencies targeted for compensation. This is achieved by broadening the bandwidth, which in turn is accomplished by diminishing the characteristic impedance described by the relation,

$$Z = \sqrt{L_f C_f} \tag{24}$$

Adjusting the characteristic impedance, as per Equation 24, can be achieved by increasing C_f while simultaneously reducing L_f. However, it is worth noting that an elevated value of C_f introduces a substantial capacitive reactive current that flows through the HAPF.

This outcome not only influences the power factor of the source but also elevates the current rating. Conversely, reducing the magnitude of L_f amplifies the switching ripple within the HAPF current. In essence, the selection of appropriate L_f and C_f values necessitate a careful balance between multiple factors. This intricate trade-off is encompassed within the following set of inequalities:

- In the scenario where the filter capacitor value's upper limit is determined to maintain a capacitive reactive current that is merely 10% of the rated load current, the impact on the grid is notably minimal. This effect holds even in the presence of a unity power factor for the load feeder. However, this condition demonstrates a slight 0.5% degradation for the grid but proves to be beneficial in cases where a lagging power factor is encountered. The following equation expresses this capacitive reactive current,

$$I_{conv(fund)} = \frac{V_{grid}}{\left|\left(2\pi f L_f - \frac{1}{2\pi f C_f}\right)\right|} \leq 0.1 I_L \tag{25}$$

Here, V_{grid} signifies the rated phase-to-neutral grid voltage, I_L corresponds to the rated load current, and f represents the nominal grid frequency.

- Opting for a reduced value of L_f amplifies the switching voltage fluctuations occurring at the PCC. Consequently, the proportion of switching-induced voltage oscillations at the PCC in relation to the terminal of the APF is expressed as:

$$\frac{V_{sw(PCC)}}{V_{sw(APF)}} = \frac{L_s}{L_s + L_f} \tag{26}$$

Here, the source inductance is specified as L_s.

3.4.3. HAPF DC Voltage

The fundamental frequency of the grid voltage is typically unaffected by the HAPF. The primary function of the HAPF is to target and eliminate harmonic currents generated by nonlinear loads. These harmonic currents, which are multiples of the fundamental frequency, distort the voltage waveform and negatively impact the power quality. The HAPF generates counteracting currents that cancel out the harmonic currents produced by the loads. This is done in real time, and the APF injects currents with precisely controlled magnitudes and phases to neutralize the harmonic components. The injection of current by the APF results in the appearance of a harmonic voltage across PPF, which is estimated as,

$$v_{filter} = R_f i_{conv} + L_f \frac{di_{conv}}{dt} + \frac{1}{C_f} \int i_{conv}\, dt \tag{27}$$

Here, the passive filter resistance is R_f, while the DC bus voltage is established at a stable 600V that proves ample for generating the requisite harmonic voltage v_{filter}. The peak value of HAPF current is specified as I_{conv}.

3.4.4. DC Bus Ripple Current and Capacitance

The average DC current tends to be zero in a balanced system. However, the switching actions render the instantaneous current passing through the capacitor to remain non-zero. Deriving the exact analytical expression for the DC current is intricate due to the complexities introduced by these switching actions. The expression for the rms value of the ripple current is,

$$I_{c(rms)} = \frac{I_{conv}}{2} \tag{28}$$

In the scenario of an extremely worst-case design, taking into account the ripple current frequency as the 6th harmonic, the determination of C_{dc} is,

$$C_{dc} = \frac{I_{c(rms)}}{3\sqrt{2}\pi f \Delta V_{dc(pk-pk)}} \tag{29}$$

Here, the peak-to-peak ripple DC voltage is specified as $\Delta V_{dc(pk-pk)}$. The HAPF working is controlled using RNN assisted DQ theory-based control approach.

3.5. RNN Assisted DQ Theory-Based Control of HAPF

The DQ theory, also known as Park's transformation or Clarke's transformation, is a mathematical technique used to convert three-phase signals into two orthogonal components: D (Direct) and Q (Quadrature). This transformation simplifies the control of three-phase systems in a rotating reference frame. In the context of HAPF control, the DQ theory can be applied to extract the harmonic components from the measured three-phase currents. The DQ reference currents are generated based on the desired harmonic compensation and power factor correction.

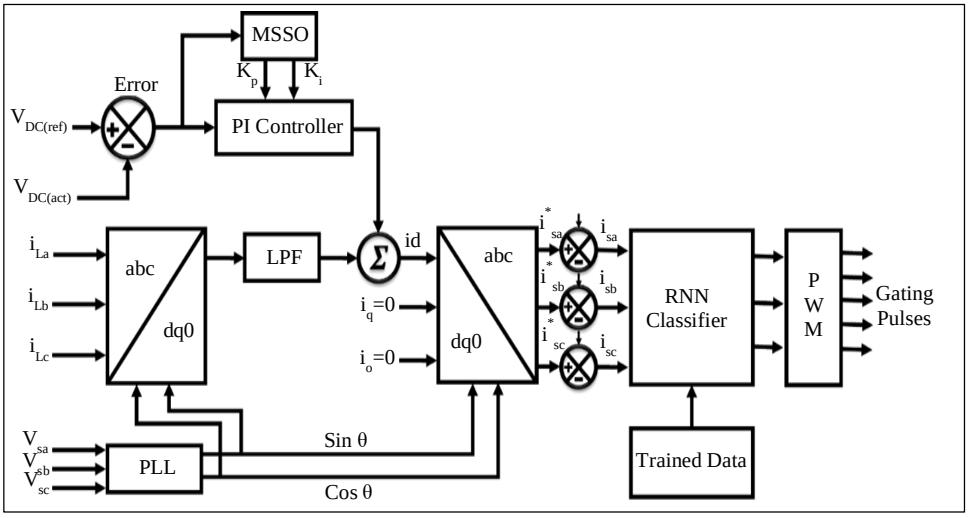

Fig. 5 RNN-assisted DQ theory-based control of HAPF

The structure of RNN-assisted DQ control is showcased in Figure 5. The transformation equations for DQ theory are as follows:

3.5.1. D-Axis Component (i_d):

$$i_d = i_a * cos(\theta) + i_b * cos(\theta - 2\pi/3) + i_c * cos(\theta + 2\pi/3) \quad (30)$$

3.5.2. Q-Axis Component (i_q):

$$i_q = -i_a * sin(\theta) - i_b * sin(\theta - 2\pi/3) - i_c * sin(\theta + 2\pi/3) \quad (31)$$

Where: i_a, i_b, i_c are the measured three-phase currents. θ is the angle of the rotating reference frame.

The RNN classifier serves as an intelligent system trained to discern and eliminate harmonics from the reference current signal, thus producing an output devoid of harmonic distortions. This process unfolds through a series of systematic steps. Firstly, a comprehensive dataset containing labeled reference current signals is assembled to train the RNN classifier.

This dataset encompasses a range of scenarios, capturing diverse operational conditions and instances of harmonic interference. During the training phase, the RNN's objective revolves around internalizing the intricate patterns distinctive to harmonics and non-harmonics within the reference current signals. Each input signal is sequentially presented to the RNN, allowing it to progressively analyze and grasp the sequential dependencies, leading to predictions regarding the presence of harmonics.

The heart of the training process lies in a defined loss function, which quantifies the disparity between the RNN's predictions and the actual labels - whether the component is deemed harmonic or non-harmonic. This loss function guides an optimization algorithm, which fine-tunes the RNN's internal parameters, refining its predictive abilities. Once the RNN is proficiently trained, it is deployed in real time to process new reference current signals.

As each new signal is inputted, the RNN conducts ongoing predictions, offering insights into the presence of harmonics at successive timesteps. When the RNN identifies a harmonic component, it undertakes the remarkable feat of adapting the output to eliminate the harmonic content meticulously. As a consequence of this harmonics removal process, the output signal from the RNN emerges as a remarkably improved reference current-liberated from the encumbrance of harmonics. This harmonics-free reference current signal, now cleansed of any distortions, stands as an optimal input for the Pulse Width Modulation (PWM) generator, which steers the Hybrid Active Power Filter (HAPF) operation.

Table 1. Parameter specifications of RNN

Parameter	Value
Number of Hidden Layers	2
Number of LSTM Units	128
Activation Function	Tanh
Dropout	0.2
Learning Rate	0.001
Optimizer	Adam
Loss Function	Mean Squared Error (MSE)
Number of Training Epochs	50
Batch Size	32
Dataset Size	1000
Prediction Threshold	0.5

4. Results and Discussions

The power produced by solar cells is improved using an I-Luo converter before being converted to AC power using a single-phase VSI system and the MATLAB application. The parameters needed for the PV system and the I-Luo converter are shown in Table 2. Both the MSSO and PI controlling techniques are displayed, and an evaluation is provided.

Table 2. Parameter specifications

Parameters	Rating
PV System	
Peak power	10 KW
V_{OC}, I_{SC}, V_{SC}	22.6V, 41.6A, 12V
Number of panels	20, 500W
I-Luo Converter	
L_1, L_2	$1mH$
C_1, C_2	$4.7\mu F$
C_0	$22{,}00\mu F$
AC Source	
Inductance	$10mH$
Resistance	100Ω
Nonlinear Load	
Voltage	$330 - 470V$
Current	$0 - 30A$

The characteristics of the solar PV system in terms of temperature and radiation are shown in Figure 6. After the surface temperature of the sun rises, it is observed that the temperature climbs from its initial starting point of 25°C to an average temperature of 35°C. Similar to this, the panel maintains its initial irradiation level of 800W/sq m. However, after 0.2s, due to an increase in temperature, it reaches 1000W/sq m, providing enough supply to the converter input.

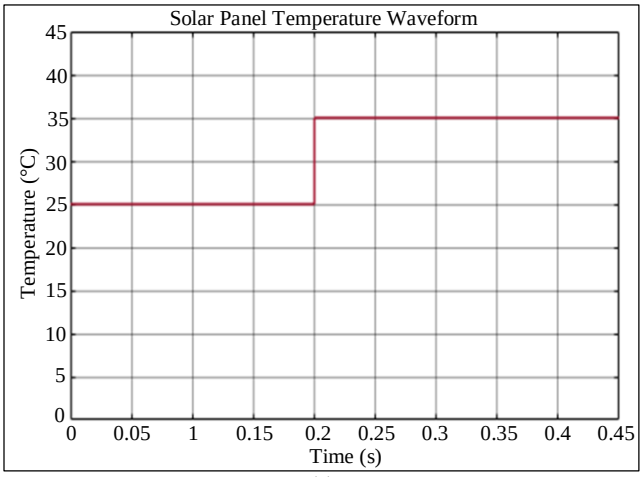

(a)

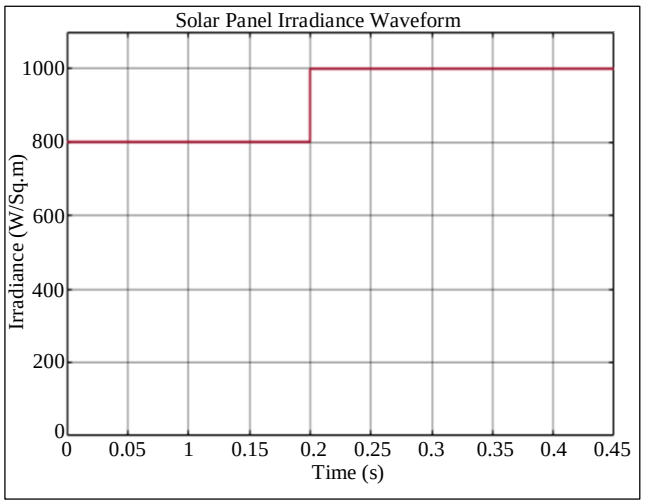

(b)

Fig. 6 PV waveform (a) Temperature, and (b) Irradiance.

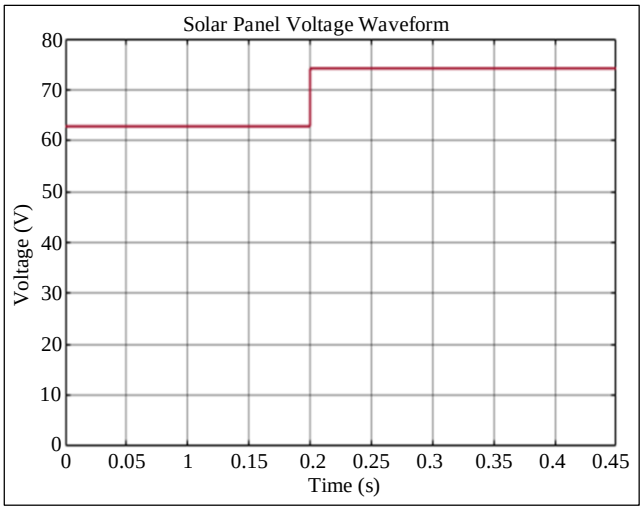

(a)

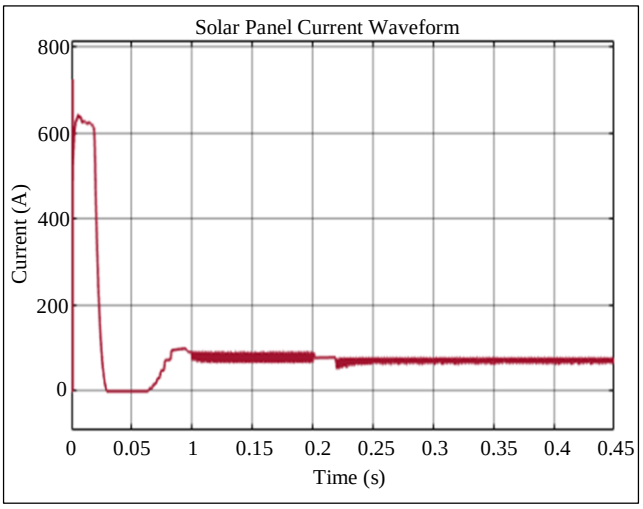

(b)

Fig. 7 PV waveform (a) Voltage, and (b) Current.

Figure 7 displays the waveform of the electrical voltage and current coming from the solar panel and going to the I-Luo converter. An initial input voltage of 62V is attained and held for 0.2 seconds, after which time the voltage rises to 75V and remains constant due to an increase in the PV parameter. According to this, a constant current level of 80A is obtained after 0.22 seconds of the PV current's first phase's peak increase.

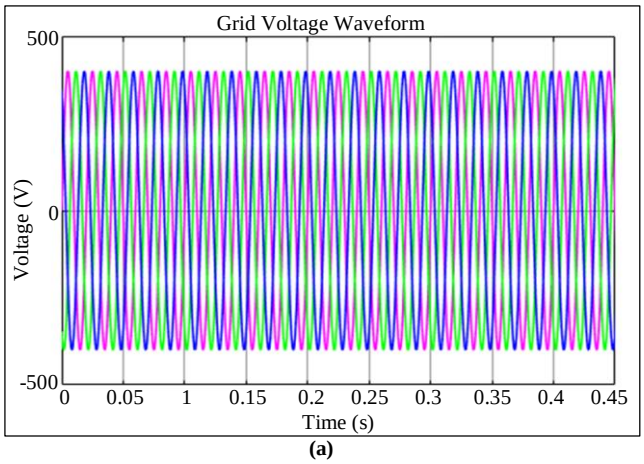

(a)

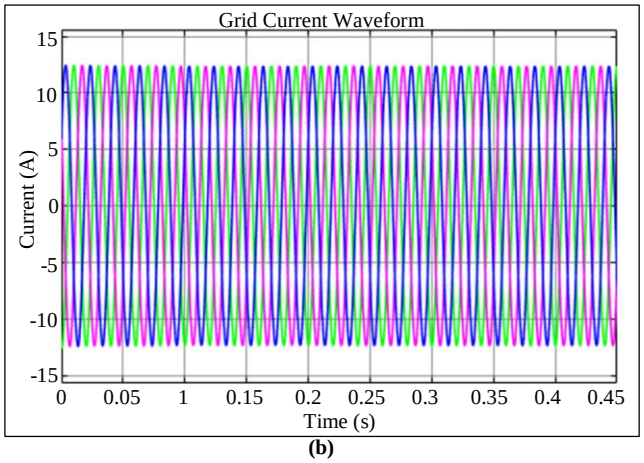

(b)

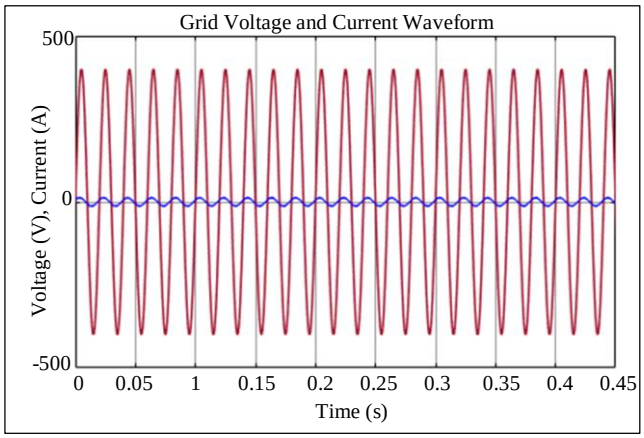

(c)

Fig 8. 3Φ Grid (a) Voltage, (b) Current, and (c) Voltage and current.

The voltage and current waveforms of a 3Φ grid are depicted in Figures 8(a) and 8(b), which indicate different kinds of electrical energy. These waveforms offer a constant and constant flow of power with successful power transmission, efficient operation of electrical equipment, and maintenance of a reliable system due to regulated voltage and current.

The waveforms of reactive and real power are shown in Figure 9 as examples. It has been noted that the genuine power eventually stabilizes at roughly 8700W after initially going through a few minor changes. Reactive power, on the other hand, generates voltage and current phase changes and is the initial oscillating power that occurs from the presence of inductive or capacitive

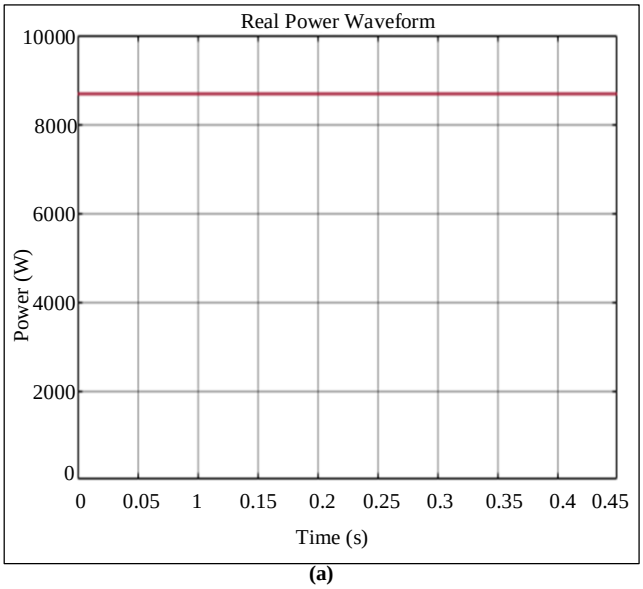

(a)

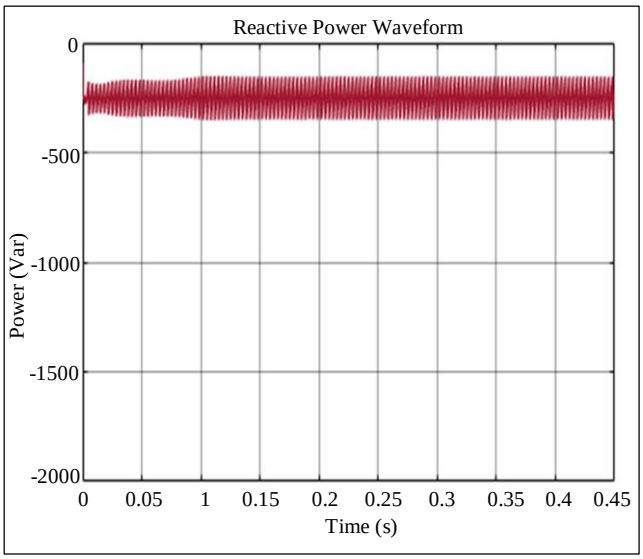

(b)

Fig. 9 (a) Real, and (b) Reactive power waveform.

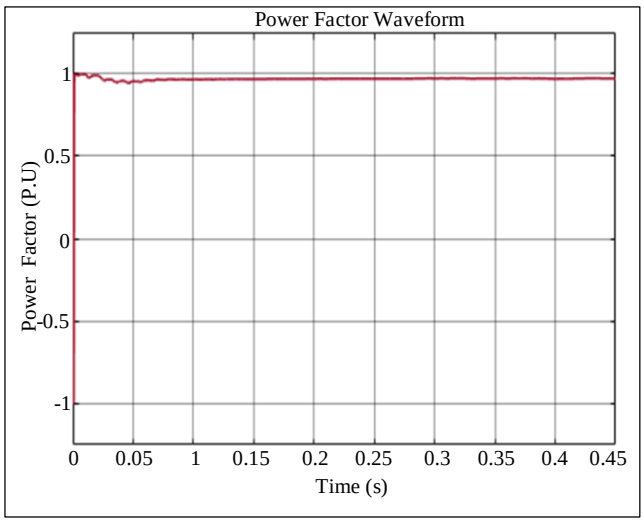

Fig. 10 Power factor waveform

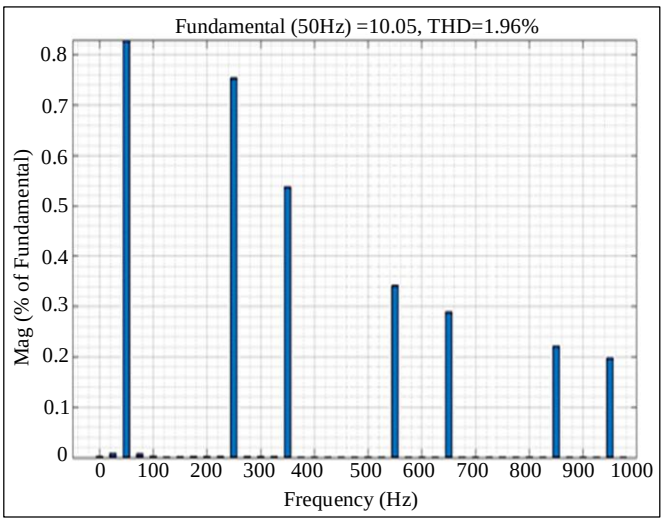

Fig. 11 Performance measure of THD value

The graph above displays an analysis of the grid-connected PV system's THD effectiveness and displays 1.96%. This shows that the PV system is producing power that is pure and of superior quality, with little harmonic distortion entering the grid. Additionally, it guarantees improved grid compatibility, lowering the danger of breakdowns and grid instabilities.

5. Conclusion

Harmonics are being introduced into power system networks by the expanding usage of nonlinear devices, which causes distortion in the current and voltage signals and injury to Power Distribution Systems (PDS). As a result, it is crucial to get rid of harmonics in power systems. The HAPF based on RNN is an effective techno-economical solution that reduces harmonics and enhances the power factor in PDS.

For PF re-regulation at the mains in steady state and at abruptly varying ranges of operational voltages, an I-Luo converter for PV systems is devised, and the PI-controller's settings are adjusted using the MSSO. The simulation results demonstrated a steady response and efficiency for the suggested controller. These values allowed for reaching the target speed with a quick and stable reaction. THD effectiveness achieves 1.96% which shows little harmonic distortion entering the grid.

References

[1] M.R. Elkadeem et al., "Optimal Planning of Renewable Energy-Integrated Distribution System Considering Uncertainties," *IEEE Access*, vol. 7, pp. 164887-164907, 2019. [CrossRef] [Google Scholar] [Publisher Link]

[2] Shichao Liu, Xiaoyu Wang, and Peter Xiaoping Liu, "A Stochastic Stability Enhancement Method of Grid-Connected Distributed Energy Storage Systems," *IEEE Transactions on Smart Grid*, vol. 8, no. 5, pp. 2062-2070, 2017. [CrossRef] [Google Scholar] [Publisher Link]

[3] Dang-Minh Phan, and Hong-Hee Lee, "Interlinking Converter to Improve Power Quality in Hybrid AC–DC Microgrids with Nonlinear Loads," *IEEE Journal of Emerging and Selected Topics in Power Electronics*, vol. 7, no. 3, pp. 1959-1968, 2019. [CrossRef] [Google Scholar] [Publisher Link]

[4] Shiying Zhou et al., "An Improved Design of Current Controller for LCL-Type Grid-Connected Converter to Reduce Negative Effect of PLL in Weak Grid," *IEEE Journal of Emerging and Selected Topics in Power Electronics*, vol. 6, no. 2, pp. 648-663, 2018. [CrossRef] [Google Scholar] [Publisher Link]

[5] Bhukya Nageswar Rao et al., "Development of Cascaded Multilevel Inverter Based Active Power Filter with Reduced Transformers," *CPSS Transactions on Power Electronics and Applications*, vol. 5, no. 2, pp. 147-157, 2020. [CrossRef] [Google Scholar] [Publisher Link]

[6] Pravat Kumar Ray, "Power Quality Improvement Using VLLMS Based Adaptive Shunt Active Filter," *CPSS Transactions on Power Electronics and Applications*, vol. 3, no. 2, pp. 154-162, 2018. [CrossRef] [Google Scholar] [Publisher Link]

[7] Silvia Costa Ferreira et al., "Finite Control Set Model Predictive Control for Dynamic Reactive Power Compensation with Hybrid Active Power Filters," *IEEE Transactions on Industrial Electronics*, vol. 65, no. 3, pp. 2608-2617, 2018. [CrossRef] [Google Scholar] [Publisher Link]

[8] Sachin Devassy, and Bhim Singh, "Control of a Solar Photovoltaic Integrated Universal Active Power Filter Based on a Discrete Adaptive Filter," *IEEE Transactions on Industrial Informatics*, vol. 14, no. 7, pp. 3003-3012, 2018. [CrossRef] [Google Scholar] [Publisher Link]

[9] M. Ehsan Raoufat, Alireza Khayatian, and Aslan Mojallal, "Performance Recovery of Voltage Source Converters with Application to Grid-Connected Fuel Cell DGs," *IEEE Transactions on Smart Grid*, vol. 9, no. 2, pp. 1197-1204, 2018. [CrossRef] [Google Scholar] [Publisher Link]

[10] Hamed Bizhani et al., "A Grid-Connected Smart Extendable Structure for Hybrid Integration of Distributed Generations," *IEEE Access*, vol. 7, pp. 105235-105246, 2019. [CrossRef] [Google Scholar] [Publisher Link]

[11] Seema Kewat, and Bhim Singh, "Grid Synchronization of WEC-PV-BES Based Distributed Generation System Using Robust Control Strategy," *IEEE Transactions on Industry Applications*, vol. 56, no. 6, pp. 7088-7098, 2020. [CrossRef] [Google Scholar] [Publisher Link]

[12] Sunaina Singh et al., "Seamless Control of Solar PV Grid Interfaced System with Islanding Operation," *IEEE Power and Energy Technology Systems Journal*, vol. 6, no. 3, pp. 162-171, 2019. [CrossRef] [Google Scholar] [Publisher Link]

[13] Daolian Chen, and Hanchao Zeng, "A Buck Type Multi-Input Distributed Generation System with Parallel-Timesharing Power Supply," *IEEE Access*, vol. 8, pp. 79958-79968, 2020. [CrossRef] [Google Scholar] [Publisher Link]

[14] Behdad Faridpak et al., "Developing a Super-Lift Luo-Converter with Integration of Buck Converters for Electric Vehicle Applications," *CSEE Journal of Power and Energy Systems*, vol. 7, no. 4, pp. 811-820, 2020. [CrossRef] [Google Scholar] [Publisher Link]

[15] Alok Kumar Mishra et al., "PSO-GWO Optimized Fractional Order PID Based Hybrid Shunt Active Power Filter for Power Quality Improvements," *IEEE Access*, vol. 8, pp. 74497-74512, 2020. [CrossRef] [Google Scholar] [Publisher Link]

[16] Touqeer Ahmed Jumani et al., "Swarm Intelligence-Based Optimization Techniques for Dynamic Response and Power Quality Enhancement of AC Microgrids: A Comprehensive Review," *IEEE Access*, vol. 8, pp. 75986-76001, 2020. [CrossRef] [Google Scholar] [Publisher Link]

[17] Patan Javeed et al., "SEPIC Converter for Low Power LED Applications," *Journal of Physics: Conference Series*, vol. 1818, pp. 1-11, 2021. [CrossRef] [Google Scholar] [Publisher Link]